THE JOURNAL OF PHYSICAL CHEMISTRY B

Article

pubs.acs.org/JPCB

Excited-State Dynamics of Rhodamine 6G in Aqueous Solution and at the Dodecane/Water Interface

Marina Fedoseeva, Romain Letrun, and Eric Vauthey*

Department of Physical Chemistry, University of Geneva, 30 Quai Ernest-Ansermet, Geneva, Switzerland

Supporting Information

ABSTRACT: The excited-state dynamics of rhodamine 6G (R6G) has been investigated in aqueous solution using ultrafast transient absorption spectroscopy and at the dodecane/water interface using the femtosecond time-resolved surface second harmonic generation (SSHG) technique. As the R6G concentration exceeds ca. 1 mM in bulk water, both R6G monomers and aggregates are excited to a different extent when using pump pulses at 500 and 530 nm. The excited-state lifetime of the monomers is shortened compared to dilute solutions because of the occurrence of excitation energy transfer to the aggregates, which themselves decay nonradiatively to the ground state with a ca. 70 ps time constant. At the dodecane/water interface, both monomers and aggregates contribute to the SSHG signal to an extent that depends on the bulk concentration, the pump and probe wavelengths, and the polarization of probe and signal beams. The excited-state lifetime of the monomers at the interface is of the order of a few picoseconds even at bulk concentrations where it is as large as several nanoseconds. This is explained by the relatively high interfacial affinity of R6G that leads to a large interfacial concentration, favoring aggregation and thus rapid excitation energy transfer from monomers to aggregates.

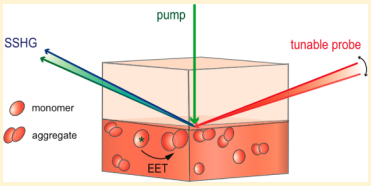

INTRODUCTION

The omnipresence and definite importance of liquid interfaces in many areas of science and technology[1−3] have attracted considerable interest from spectroscopists over the past decades.[4−24] Whereas many established techniques exist for characterizing solid surfaces with atomic resolution, the situation is different for liquid interfaces, which are typically a few nanometers thick.[25,26] Primarily due to surface disorder, capillary waves, and volatility of liquids, our knowledge on the detailed molecular structure of these interfaces has been primitive until the development of nonlinear optical spectroscopic techniques combined with molecular dynamics simulations.[27−30] Additionally, the extremely small number of molecules occupying the interfaces relatively to those making up the bulk phases constitutes a major challenge for their quantitative characterization even when using spectroscopic probes.

Second-order nonlinear spectroscopic techniques, such as surface sum frequency generation and surface second harmonic generation (SSHG), are powerful methods to address these challenges.[6,21,31] Besides being nonzero at the interface between two isotropic media, the second-order nonlinear optical susceptibility is also frequency dependent, allowing a spectroscopic identification of the interfacial molecules.

Our main interest is to understand how the photophysical and photochemical properties of molecules adsorbed at an interface differ from those of the same molecules dissolved in the bulk phases. Indeed, because of the anisotropy of forces at the interface, the adsorbed molecules have a non-random orientation and experience a different environment than those in the bulk phases. Investigating the excited-state dynamics of these molecules yields precious information on the properties of the interfacial region and is important for the development of interfacial photochemistry.[32] Furthermore, understanding properties of dye molecules in aqueous solutions at hydrophobic surfaces, such as orientation or aggregation, is particularly relevant for many practical applications in areas like e.g. the textile and fiber industry.[33,34]

We present here a comparative investigation of the excited-state dynamics of rhodamine 6G in aqueous solution and at the dodecane/water interface. Although R6G is being extensively used in areas as diverse as laser technology and life sciences,[35,36] there still is no fully conclusive study, to our knowledge, on its ultrafast excited-state dynamics, neither in bulk nor at liquid interfaces.

The fluorescence quantum yield of R6G is known to decrease with increasing concentration because of self-quenching.[37] This has been shown to be due to the formation of nonemissive aggregates that quench the excited state of the monomers by excitation energy transfer.[38−40] Whereas in methanol the decrease of the monomer fluorescence quantum yield takes place above ca. 10^{-2} M,[38] in water, it is observed when exceeding concentrations as low as 10^{-5} M.[40] According to Penzkofer and co-workers, the aggregates are dimers with an electronic absorption spectrum largely overlapping that of the monomer but with a maximum at ca. 500 nm vs 530 nm for the monomer.[38,40,41] On the basis of the absorption cross section of the dimer and its fluorescence quantum yield, the same authors estimated the excited-state lifetime of the dimers

Received: February 27, 2014
Revised: April 25, 2014
Published: April 28, 2014

   dx.doi.org/10.1021/jp502058e | J. Phys. Chem. B 2014, 118, 5184−5193

to amount to a few picoseconds. Subsequent investigations also pointed out the formation of trimers and tetramers in highly concentrated aqueous solutions.[39,42]

Although several studies on R6G adsorbed at liquid interfaces have been reported,[43−47] those dedicated to its excited-state dynamics are still very scarce. Time-resolved (TR) SSHG measurements on R6G adsorbed at the silica/water interface point to a ground-state recovery taking place on the ca. 100 ps time scale.[48] Several hypotheses were proposed to explain this effect, e.g., dimer dissociation to the ground state or energy transfer from excited monomers, but no definitive conclusion could be drawn.[48] Using the same technique, Eisenthal and co-workers could show that the reorientational dynamics of R6G at the air/water interface is significantly slower than that in bulk water.[49] Finally, the excited-state lifetime of R6G at the decaline/methanol interface measured using the evanescent transient grating technique was found to be twice as small as that in bulk methanol at the same concentration.[50,51] However, this technique, like total internal reflection fluorescence,[52] is not intrinsically selective to the interface as it probes a layer close to the interface that is several hundreds of nanometers thick, and thus dye populations in both the interfacial and the bulk regions contribute to the signal.

We report here on the ultrafast excited-state dynamics of R6G in bulk water and at the dodecane/water interface using a combination of femtosecond transient absorption (TA) and TR-SSHG. By using various R6G concentrations, different excitation wavelengths, and broadband or tunable probing, R6G monomers and aggregates could be spectroscopically distinguished in both transient absorption and TR-SSHG measurements.

EXPERIMENTAL SECTION

Samples. The aqueous solutions of R6G chloride (Acros Organics) were prepared at bulk concentrations of 0.1, 1, and 10 mM for both TA and TR-SSHG experiments by dissolving the dye in deionized water. In all TR-SSHG experiments, the upper organic phase was dodecane (Acros Organics, >99%). The pH of the samples was between 4 and 8 depending on the R6G concentration. The steady-state absorption, fluorescence spectra, and lifetime of R6G were found to be insensitive to the change of pH in this range. The pH was ensured to remain unchanged before and after the measurements.

For the stationary and transient absorption as well as for the time-resolved fluorescence experiments, the 0.1, 1, and 10 mM R6G solutions were placed in 1 mm, 10 μm, and 1 μm thick quartz cells, respectively. For the steady-state fluorescence measurements, the sample was located in a 10 mm quartz cell. For the TR-SSHG experiments an 4 × 4 × 4 cm^3 optical glass cell was used.

Steady-State Spectroscopy. Electronic absorption and emission spectra were recorded on a Cary 50 spectrophotometer and a Cary Eclipse spectrofluorometer, respectively.

Time-Resolved Fluorescence. Fluorescence lifetime measurements were performed using the time-correlated single photon counting (TCSPC) technique with a setup similar to that described in detail in refs 53 and 54. Excitation was carried out at 470 nm and 10 MHz repetition rate using a laser diode (Picoquant, LHD-D-C-470). The laser pulse duration was 60 ps, and the full width at half-maximum (fwhm) of the instrument response function (IRF) was about 200 ps. The fluorescence was collected at magic angle after passing through a 570 nm interference filter.

Transient Absorption Spectroscopy. The TA setup has been described in detail elsewhere.[55,56] Excitation was performed at 500 or 530 nm with a home-built two-stage noncollinear optical parametric amplifier. The irradiance on the sample was about 1 mJ/cm^2. The polarization of the probe pulses was at magic angle relative to that of the pump pulses. All spectra were corrected for the chirp of the white-light probe pulses. The IRF was ca. 150 fs fwhm. In order to avoid photodegradation, the R6G solutions were either continuously stirred by N_2 bubbling (for 1 mm cell) or continuously moved in the plane perpendicular to the probe beam (for 10 and 1 μm cells). The sample absorbance at the excitation wavelength was between 0.8 and 1. Because of the motion of the cell during the measurements, scattering of the pump beam could not be avoided, and thus the TA spectra were in many cases contaminated in the 480−550 nm region, which coincides with the spectral signature of the ground-state bleach. Apart from distorting the spectra, this scattering introduces substantial high-frequency noise in the time profiles measured in this region. In order to eliminate this noise, the TA data recorded at each R6G concentration and excitation wavelength were analyzed globally using a routine based on the matrix reconstruction algorithm written in MATLAB (The MathWorks Inc.).[57] The experimental TA spectra could, in all cases, be well reproduced with a biexponential function. To illustrate the robustness of the procedure, Figure 1 shows a comparison of the original

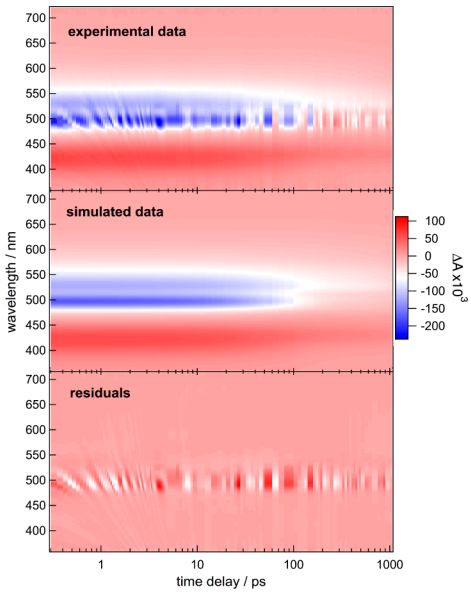

Figure 1. Transient absorption data recorded after 500 nm excitation of a 1 mM R6G aqueous solution (top), simulated data (middle, see text for details), and difference between experimental and simulated data (bottom).

experimental data and of the corresponding simulated data, together with the associated residuals map. Careful inspection of the latter reveals only high-frequency noise caused by the scattering in the pump pulse region. The fact that the residuals maps do not exhibit any structured features in both time and spectral domains ensures a good recovery of the spectrotemporal dynamics over the whole data set. Qual-

dx.doi.org/10.1021/jp502058e | J. Phys. Chem. B 2014, 118, 5184−5193

itatively similar residuals maps as shown in Figure 1 were obtained for all TA spectra. Only these simulated TA spectra will be presented here, whereas the original ones are shown in Figure S1 (Supporting Information).

Surface Second Harmonic Generation. Two different TR-SSHG setups, whose detailed description can be found elsewhere,[58−60] have been used. In the first one,[58,59] the pump pulses (∼50 fs, 1 μJ at the interface) were generated by a noncollinear optical parametric amplifier (NOPA, Clark-MXR), had circular polarization, and were focused onto the interface from the top using a combination of spherical and cylindrical lenses (Figure 2). Probing was achieved at total

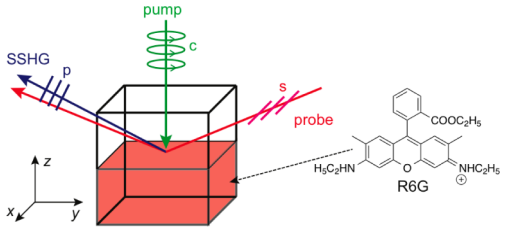

Figure 2. Beam geometry and polarization (for the *zxx* configuration) used in the TR-SSHG experiment and structure of R6G.

internal reflection geometry with 800 nm pulses (∼200 fs, 1 kHz, ∼100 nJ at the interface). The SSHG signal at 400 nm was collected with a lens, filtered out from unwanted scattering with a Schott BG23 color filter, and detected with a multipixel photon counter avalanche photodiode (S-10362-11-050U, Hamamatsu), located at the exit of a monochromator. The output signal was processed with a boxcar gated integrator and averager module before being digitized and stored on a computer. In the second setup,[60] the pump pulses (∼80 fs, 1−2 μJ at the interface) were generated with a noncollinear optical parametric amplifier (TOPAS White, Light Conversion), whereas the probe pulses (∼100 fs, 200 nJ at the interface) were produced with a collinear optical parametric amplifier (TOPAS C, Light Conversion). The beam geometry and SSHG signal collection were similar to the above-described setup (Figure 2). The signal was focused onto the entrance slit of a Czerny-Turner spectrograph (Shamrock 163, Andor) equipped with a multipixel cooled CCD camera (Newton 920, Andor). The illuminated pixels were vertically binned, summed over the wavelength range of interest, and the resulting value stored on a computer.

The nonresonant contribution to the SSHG signal measured without R6G in the aqueous phase was found to be negligibly small. As a consequence, the SSHG signal measured with R6G has a purely electronic resonant character, and its intensity is proportional to the square modulus of the relevant tensor element of the second-order nonlinear susceptibility tensor, $\vec{\vec{\chi}}^{(2)}$. Two different sets of polarizations of the probe and signal fields were used in order to examine two of the three independent nonvanishing elements of $\vec{\vec{\chi}}^{(2)}$:[61] (1) In the *zxx* configuration, the probe field polarization is perpendicular (s) to the plane of incidence, whereas the parallel (p) polarization component of the SH signal field is measured (Figure 2). The signal intensity is proportional to $|\chi^{(2)}_{zxx}|^2$. (2) In the *xxz* configuration, the probe field polarization is at 45°and the perpendicular polarization component of the SH signal field is recorded. The signal intensity is proportional to $|\chi^{(2)}_{xxz}|^2 = |\chi^{(2)}_{xzx}|^2$.

On the other hand, with the beam geometry used here, there is no set of polarizations allowing the third nonzero tensor element, $\chi^{(2)}_{zzz}$, to be measured independently.

The TR-SSHG profiles were processed by first taking the square root of the measured SSHG intensity and then normalizing, so that the signal is zero at negative pump−probe delays and is equal to −1 at the strongest photoinduced signal depletion. The resulting signal intensity, $S(t)$, is then proportional to the photoinduced population changes. Analysis of these time profiles was performed by nonlinear least-squares fitting using the Levenberg−Marquardt algorithm, as implemented in Igor Pro (v. 6.3, Wavemetrics Inc.).[60]

Stationary SSHG spectra were recorded using the second setup described above. This was done by scanning the probe wavelength from 790 to 1070 nm by steps of 10 nm. At each probe wavelength, the SSHG intensity was detected within a spectral window of the CCD camera corresponding to half the probe wavelength. The probe pulse energy at the sample position was kept constant at 1 μJ.

RESULTS AND DISCUSSION

Steady-State Measurements. Figure 3 shows electronic absorption spectra of R6G in water measured at different

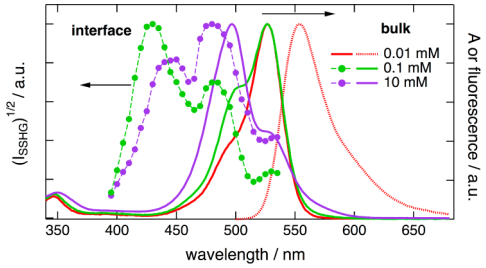

Figure 3. Stationary SSHG spectra measured with R6G at the dodecane/water interface (full circles), electronic absorption (color solid lines), and emission spectra (red dotted line) measured with aqueous solutions of R6G at different concentrations.

concentrations. At low concentration, the spectrum is dominated by the $S_1 \leftarrow S_0$ band culminating at 530 nm with a shoulder around 500 nm originating from a vibronic transition. A weaker band arising from the $S_3 \leftarrow S_0$ transition can be observed at ca. 350 nm. The $S_2 \leftarrow S_0$ transition is symmetry forbidden and predicted to be around 425 nm.[62] However, it is two photon allowed and clearly visible in the two-photon excitation fluorescence spectrum of R6G.[63] Upon increasing concentration, the relative absorbance at 530 and 500 nm changes, and above ca. 0.5 mM, the maximum of the low-energy band is at 500 nm and the original 530 nm maximum evolves into a shoulder. This change is well documented and arises from the formation of aggregates, mostly H dimers, although larger aggregates, trimers and tetramers, are also present above ca. 1 mM.[40,42,64] The 350 nm band is less affected by the increased R6G concentration and exhibits mostly a slight red-shift and broadening of its low-energy side.

Figure 3 also shows stationary SSHG spectra measured with R6G at the dodecane/water interface at 0.1 and 10 mM upon probing between 790 and 1070 nm using the *zxx* configuration. At the lowest concentration, the SSHG spectrum is dominated by a band centered at ca. 430 nm.

dx.doi.org/10.1021/jp502058e | J. Phys. Chem. B 2014, 118, 5184−5193

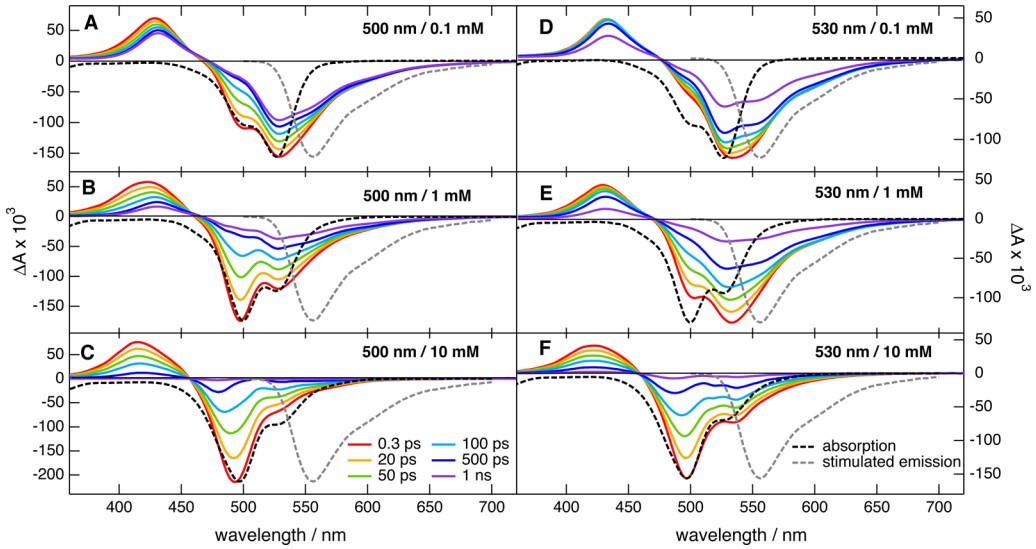

Figure 4. Simulated transient spectra obtained from a global analysis of the transient absorption spectra measured at different time delays after 500 (A–C) or 530 nm excitation (D–F) of aqueous R6G solutions, and intensity-scaled absorption and stimulated emission spectra, calculated by multiplying the stationary fluorescence intensity by λ^4 [66] (black and gray dashed lines).

This band coincides well with the two-photon absorption spectrum of R6G,[63] pointing to a possible enhancement of the SSHG intensity via a two-photon resonance with the $S_2 \leftarrow S_0$ transition of R6G.

At the highest concentration, the most intense band peaks at ca. 485 nm and most probably arises from aggregates. Whereas the absorption maximum of R6G dimers peaks at ca. 500 nm, that of trimers and tetramers was shown to be at 485 and 475 nm, respectively.[42] The high-energy band is relatively less intense than at 0.1 mM and is shifted to 445 nm. This difference might again originate from aggregation. Finally, at all concentrations, the weakest SSHG band is at 530 nm and could be due to both monomers and aggregates, the latter exhibiting a vibronic transition at this wavelength. At 10 mM, the SSHG signal is apparently dominated by the contribution of aggregates. However, the 485 nm SSHG band indicates that, unlike in the bulk solution, aggregates are present at the interface already at concentrations as low as 0.1 mM. This points to a significantly higher dye population at the interface than in the bulk.

The signal intensity in the *xxz* configuration was too small compared to the background signal to record significant SSHG spectra.

Excited-State Dynamics of R6G in Aqueous Solution. The fluorescence dynamics of R6G in water was investigated on the subnanosecond time scale using the TCSPC technique. Up to 1 mM, the fluorescence decay is exponential and the lifetime shortens from 4.5 ns at 0.1 mM to 3.7 ns at 1 mM (Figure S2). On the other hand, the fluorescence decay at 10 mM is more complex and requires the sum of at least three exponential functions to be properly reproduced (Figure S2), the amplitude-weighted average lifetime amounting to 730 ps. This shortening is consistent with the decrease of the fluorescence quantum yield reported by Penzkofer et al. and can be accounted for by the quenching of R6G fluorescence by excitation energy transfer to aggregates,[40] which, being of H-type, are nonfluorescent. The decay at high concentration can be accounted for by the intrinsic nonexponential character of the quenching dynamics, which, as the distance and orientation between the energy donors and acceptors are neither unique nor constant in time, requires a model including non-Markovian effects to be properly described.[65]

The excited-state dynamics on a shorter time scale was then investigated by TA spectroscopy. These measurements were performed using both 530 and 500 nm pump pulses, in order to excite predominantly monomers and aggregates, respectively. The original TA spectra recorded at different R6G concentrations in water are presented in the Supporting Information (Figure S1), whereas the simulated spectra obtained with the method described above are shown in Figure 4.

These TA spectra are dominated by an intense and structured negative band above 470 nm, which can be ascribed to the bleach of the absorption, due to the depletion of the ground-state monomer and aggregate populations, as well as to the $S_1 \rightarrow S_0$ stimulated emission of the monomers. A positive band that can be assigned to an excited-state absorption is also observed below 470 nm. The shape of all these TA bands depends on both the R6G concentration and pump wavelength. At the lowest concentration investigated, i.e. 0.1 mM, the relative contribution of the stimulated emission is slightly higher upon 530 than 500 nm excitation (Figure 4A,D). Similarly, the negative band due to the depletion of the ground-state population coincides well with the steady-state absorption spectrum only when using 500 nm excitation (Figure 4A). Indeed, upon 530 nm excitation, substantial discrepancy is observed around 500 nm (Figure 4D). These two differences unambiguously confirm that the TA spectra obtained upon 530 nm pumping are dominated by the contribution of R6G monomers, whereas those measured upon 500 nm excitation contain a substantial contribution of the aggregates, which do not fluoresce and absorb predominantly at 500 nm. This pump wavelength dependence of the TA spectra is even more pronounced at 1 mM R6G (Figure 4B,E), with the negative band measured at early time delays centered at 500 or 530 nm. Similarly, the positive TA band measured at short time delays is significantly broader upon 500 nm than upon 530 nm excitation and peaks at shorter wavelength, i.e., 423 vs 430 nm. Figure 4B also shows that the shape of the TA spectra with 500 nm excitation

dx.doi.org/10.1021/jp502058e | J. Phys. Chem. B 2014, 118, 5184–5193

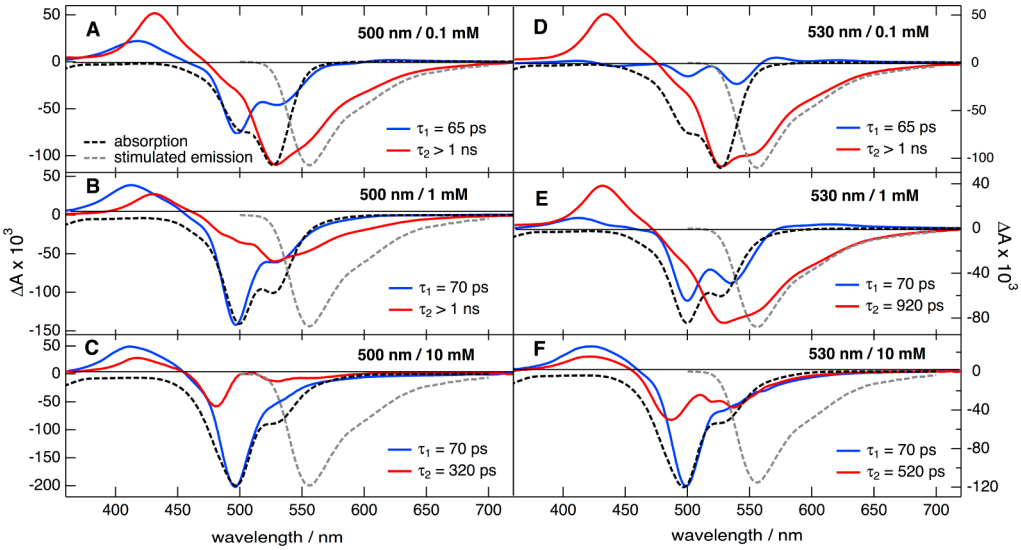

Figure 5. Decay-associated difference spectra obtained from the global analysis of the TA spectra measured with R6G in water at various concentrations upon 530 and 500 nm excitation and intensity-scaled absorption and stimulated emission spectra (black and gray dashed lines).

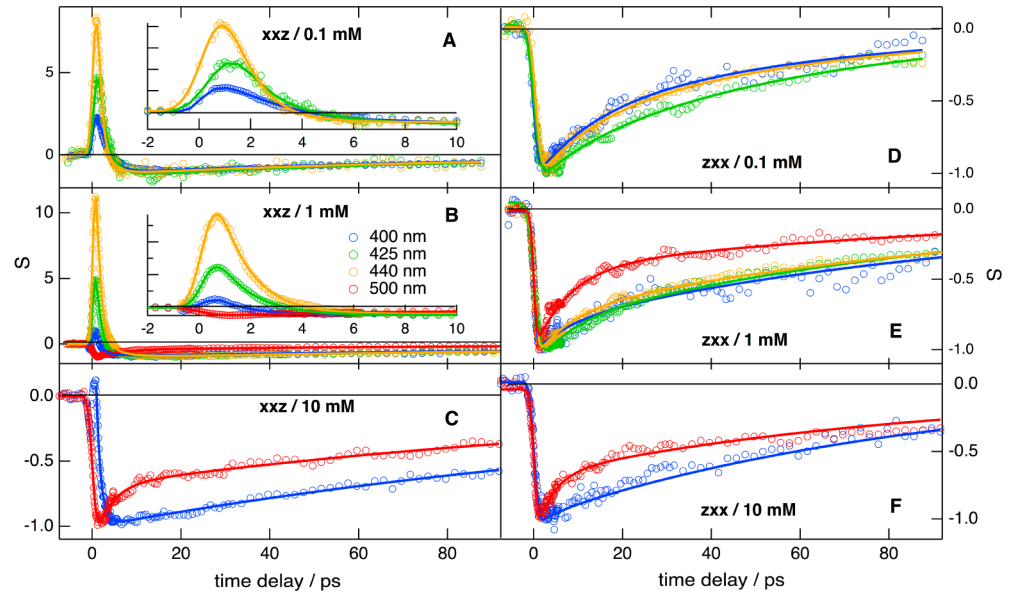

Figure 6. TR-SSHG profiles measured with R6G at the dodecane/water interface upon 530 nm excitation at different wavelengths, bulk concentrations, and polarization configurations and best multiexponential fits (solid lines). The color code is the same for all panels.

evolves substantially with time and, after about 300 ps, becomes very similar to that of the spectra recorded upon 530 nm excitation. This reveals that the spectral features of the aggregates, more visible upon 500 nm pumping, are shorter lived than those arising from the monomers. At the highest R6G concentration used here, i.e., 10 mM, the TA spectra almost no longer depend on the pump wavelength and are dominated by the contribution of the aggregates (Figure 4C,F). Only small differences can be observed, like the contribution of the stimulated emission that is only visible, although weakly, in the TA spectra measured with 530 nm excitation (Figure 4F).

Figure 5 shows the decay-associated difference spectra (DADS) and the time constants obtained from the global biexponential analysis of the TA data. The longer time constant, τ_2, is of the order of a few nanoseconds at 0.1 and 1 mM and cannot be determined accurately with the limited time window, 0−1.8 ns, of the TA experiment. It is markedly shorter, a few hundred picoseconds, at the highest R6G concentration. The relative amplitude of its DADS decreases with increasing R6G concentration as well as by going from 530 to 500 nm excitation. This DADS is characterized by a positive band at 430 nm and a negative band that, at the lower R6G concentrations, is a composite of the monomer absorption and stimulated emission spectra (Figure 5A,D). As a consequence, this longer time constant, τ_2, can be assigned to the decay of the monomer S_1 state population. The shorter time constant, τ_1, amounts to ca. 70 ps, independently of the concentration and excitation wavelength. Its DADS consists of a positive band at ca. 415 nm and of a negative band that matches well the absorption spectrum of the aggregates, with a maximum at 500 nm. Therefore, this time constant can be interpreted as the excited-state decay of the aggregates to the ground state. This lifetime is substantially larger than that of

dx.doi.org/10.1021/jp502058e | J. Phys. Chem. B 2014, 118, 5184−5193

2.2 ps reported earlier.[40] However, considering that the latter value was obtained very indirectly, i.e., from the fluorescence quantum yield and radiative rate constant of the aggregates, themselves obtained from the deconvolution of the absorption and emission spectra of R6G measured at various concentrations, this difference should not be surprising. On the other hand, this 70 ps lifetime agrees well with that of 100 ps reported for the rhodamine B dimer in water.[67]

The temporal evolution of the TA spectra can now be explained as follows: at the lowest R6G concentrations, pump light at 530 nm mostly results in the population of the monomer excited state that decays on the nanosecond time scale. Excitation of the aggregates occurs almost exclusively via excitation energy transfer (EET) quenching of the monomers and, given the low concentration and the short excited-state lifetime of the aggregates, the latter do not contribute significantly to the TA spectra. Upon 500 nm excitation, both monomers and aggregates excited states are directly populated and decay in parallel. Because of the different decay times of these two populations, the shape of the TA spectra changes with time. Typically the same behavior is observed at the medium R6G concentration at both excitation wavelengths. Finally, at the highest concentration, the two excitation channels of the aggregates, i.e., direct and via EET quenching of the monomers, are operative at both excitation wavelengths. Whereas the directly excited aggregate population decays with a ca. 70 ps time constant, the kinetics of the EET-excited aggregate population should be biexponential. As the decay of the excited aggregates is faster than the EET quenching, the kinetics should be inverted,[68] with a rise time corresponding to the decay time of the excited aggregates, i.e., 70 ps, and a decay time equal to that of the EET quenching, i.e., about 400 ps. For this reason, the τ_2 DADS obtained from the biexponential global analysis contains spectral features of both monomers and aggregates.

Excited-State Dynamics of R6G at the Dodecane/Water Interface. The interfacial excited-state dynamics of R6G was first investigated upon 530 nm excitation. Probing was performed at several wavelengths between 800 and 1000 nm and different polarization configurations to measure either the $\chi^{(2)}_{xxz}$ or the $\chi^{(2)}_{zxx}$ tensor elements. Figure 6 shows substantial dependence on the probe wavelength, concentration, and polarization. Starting with the two lower R6G concentrations, Figures 6A and 6B show that the TR-SSHG signals between 400 and 440 nm for the *xxz* configuration exhibit first a prompt rise at time zero, indicating an increase of the SSHG intensity upon excitation, followed by a fast decay to a negative value and by a subsequent slower recovery to zero. The relative intensity of the positive signal increases by going from 400 to 440 nm. On the other hand, the profile at 500 nm shows only a prompt depletion of the signal intensity and a biphasic recovery. The time profiles measured in the 400−440 nm region with the *zxx* configuration differ substantially from those recorded with the *xxz* polarization and show only an initial depletion of the signal intensity and a biphasic recovery. On the other hand, the time profiles recorded at 500 nm are very similar for both *xxz* and *zxx* configurations. Figure 6E shows that the signal recovery at this wavelength is faster than in the 400−440 nm region.

At the highest R6G concentration, the initial positive signal observed between 400 and 440 nm for the *xxz* configuration is hardly visible (Figure 6C), and apart from this weak feature, the overall aspects of the TR-SSHG profiles at both polarization configurations are similar (Figure 6C,F).

In most TR-SSHG experiments reported so far in the literature, photoexcitation of the sample causes a decrease of the SSHG intensity. This is generally due to the fact that probing is performed at a wavelength corresponding to a one- or two-photon resonance with an electronic transition from the ground state. In such case, the SSHG intensity reflects the ground-state population. As the pump pulse induces a depletion of the ground-state population, the TR-SSHG signal decreases, and its return to the initial value reflects the ground-state recovery dynamics. The increase of the SSHG intensity found here upon photoexcitation points to a resonance with a transition from an electronic excited state of R6G. The TA spectra measured with R6G in aqueous solutions (Figure 4) reveal the presence of a transient band in the 400−450 nm region ascribed to an excited-state absorption of both monomers and aggregates. According to the DADS obtained from the global analysis (Figure 5), the relative magnitude of this transition compared to that from the ground state to the first excited state is larger for the monomer than for the aggregate. As a consequence, the initial positive TR-SSHG signal is ascribed to a two-photon resonance with a $S_n \leftarrow S_1$ transition of the R6G monomer, and thus the signal intensity reflects the population of the monomer S_1 state. The diminution of this positive feature at the highest R6G concentration can be ascribed to the increased contribution of the aggregates to the SSHG signal. On the other hand, the negative component of the TR-SSHG signal that evolves on a longer time scale is assigned to the ground-state recovery of the aggregate population. The signal is most probably enhanced via a two-photon resonance with a transition from the ground state. The positive feature, ascribed to the excited-state monomers, is absent in the TR-SSHG profiles measured with the *zxx* configuration at all wavelengths investigated. This indicates that the $S_n \leftarrow S_1$ resonance enhancement discussed above is comparatively less or not operative. This can be explained by the relative orientation of the $S_n \leftarrow S_1$ transition dipole moments relative to the interface and by a poor interaction with the probe field which is parallel to the interfacial plane. With this configuration, the signal enhancement originates mostly from resonances with transitions from the monomer and aggregate ground state. This is consistent with the stationary SSHG spectra (Figure 3) that could only be properly measured using the *zxx* configuration. As a consequence, the fast and slow recovery components correspond to the repopulation of the monomer and aggregate ground state, respectively. This tentative assignment of the resonance enhancement of SSHG signal for the monomers is illustrated in Figure 7.

In principle, the observed increase of the SSHG intensity in the *xxz* configuration could arise from a perturbation of the orientational distribution of the R6G molecules upon excitation with circularly polarized light. In such case, the decay of the SSHG intensity would be due to the out-of-plane reorientational relaxation. However, such motion has been shown to occur on a much longer time scale.[49,69] Moreover, if this effect was at the origin of the increasing SSHG intensity, the TR-SSHG profiles should be independent of the probe wavelength, contrary to the observation.

To obtain more quantitative information, the TR-SSHG profiles were analyzed using a multiexponential fit. The profiles measured at a given polarization configuration and

dx.doi.org/10.1021/jp502058e | J. Phys. Chem. B 2014, 118, 5184−5193

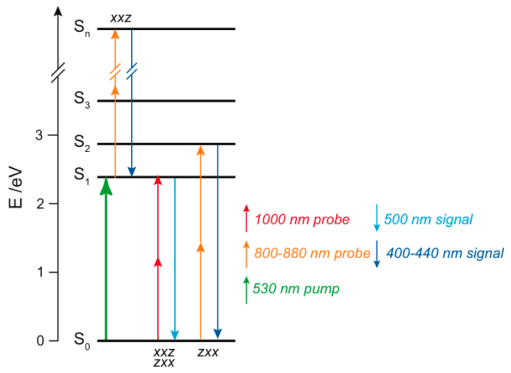

Figure 7. Energy level scheme illustrating the transitions involved in the resonance enhancement of the TR-SSHG signal from R6G monomers.

concentration but different wavelengths were analyzed globally. The sum of two to three exponential functions was required to properly reproduce the data (solid lines in Figure 6). The resulting time constants and the sign of the associated amplitudes are listed in Table 1, whereas the relative values of the amplitudes are depicted in Figure S3. At all wavelengths, polarizations, and concentrations, the largest time constant lies between 75 and 160 ps and is associated with a negative amplitude, i.e., corresponds to a recovery of the TR-SSHG intensity. This time constant is assigned to the ground-state recovery of the R6G aggregates adsorbed at the interface. The depletion of the aggregate ground-state population is due to two processes: direct and indirect excitation via EET quenching of R6G monomers. As discussed below, the latter process occurs within a few picoseconds at the interface. Given the relatively small amplitude of this component in the TR-SSHG profiles, especially with the *xxz* configuration, and the limited time window of the measurement (0−100 ps), the error on this larger time constant is considerable, i.e., ±20%. Moreover, whereas the aggregates exist mostly as dimers in the bulk phase at the concentrations investigated, the situation might be different at the interface, where a higher local concentration favors the formation of larger aggregates with probably different excited-state lifetimes. The relative contribution of these larger aggregates to the SSHG signal may depend on the polarization configuration, explaining why the longer time constant is larger in the *xxz* than in the *zxx* polarization.

All these effects could account for the difference between this largest time constant and the excited-state lifetime of the aggregates in aqueous solutions obtained from the TA measurements.

The decay of the positive TR-SSHG feature ascribed to the monomer excited-state absorption and the increase of the negative component assigned to the aggregate ground-state bleach require one or two exponential functions with time constants around 1 and 3 ps to be properly reproduced (Table 1). This process is assigned to the EET quenching of the R6G excited monomers by the aggregates. The fact that two exponential functions are needed reflects the intrinsic nonexponential character of the quenching dynamics as discussed above. Moreover, this dynamics at the interface should differ from that in the bulk because of a different dimensionality.[70,71] A quantitative discussion of the EET process is not really possible with the data available. However, the very short excited-state lifetime of the monomers at the interface points to a very efficient quenching that can be explained by a high interfacial population of R6G aggregates. The decrease of the two short time constants and, more importantly, the quasi-disappearance of the contribution of excited monomers to the TR-SSHG profiles upon increasing the bulk concentration further support this assignment. To confirm this interpretation, a TR-SSHG measurement was performed at 400 nm with even lower bulk R6G concentration, 0.05 mM. The TR-SSHG profile exhibits a relatively more pronounced positive component than at 0.1 mM with a markedly slower decay, i.e., 17 ps vs 3.5 ps (Figure S4).

The negligible contribution of excited monomers to the signal at the highest R6G concentration can be explained by the large interfacial population of aggregates that probably dominates that of the monomers. This leads not only to an important reduction of the excited monomers lifetime due to very efficient EET quenching but also to the direct excitation of aggregates at 530 nm. Such ultrafast EET quenching is not unrealistic, as Penzkofer and co-workers reported that the fluorescence lifetime of R6G in methanol, concentrated up to 600 mM, was as short as 1.5 ps.[38]

The short time constant obtained from the analysis the *zxx* time profiles is somewhat larger than those found with the *xxz* profiles. However, it also shortens with increasing R6G concentration, indicating that it should be related to the ground-state recovery of the monomer upon EET quenching. The origin of this difference between the *zxx* and *xxz* profiles is not clear but could be due to several factors, such as a different orientation of the probed molecules and thus different EET dynamics and the contribution from other processes, such as vibrational/solvent relaxation or excitation energy hopping between R6G monomers. Despite this, the time constants obtained for both configurations are qualitatively consistent.

Table 1. Time Constants, τ, Obtained from a Multiexponential Analysis of the TR-SSHG Profiles and Sign (in Parentheses) of the Associated Amplitude (+: Decay; −: Rise)

		τ/ps		
polarization	λ_{SSHG}/nm	0.1 mM	1 mM	10 mM
xxz	400−450	1.0 ± 0.1 (+)	0.9 ± 0.1 (+)	1.0 ± 0.1 (+)
		3.5 ± 0.4 (+)	2.5 ± 0.4 (+)	160 ± 35 (−)
		160 ± 35 (−)	150 ± 30 (−)	
xxz	500		5.1 ± 0.6 (−)	3.8 ± 0.8 (−)
			95 ± 20 (−)	140 ± 35 (−)
zxx	400−500	14 ± 1.5 (−)	8 ± 1 (−)	4 ± 0.5 (−)
		75 ± 15 (−)	100 ± 20 (−)	90 ± 20 (−)

dx.doi.org/10.1021/jp502058e | J. Phys. Chem. B 2014, 118, 5184−5193

In order to further ascertain the above interpretation of the TR-SSHG profiles, similar measurements were repeated using 500 nm excitation instead of 530 nm. According to the steady-state absorption spectra and the TA measurements at different R6G concentrations (Figures 3 and 4), direct excitation of the aggregates should be much more important at 500 than 530 nm. Figure 8 shows TR-SSHG profiles at 400 nm probed with the *xxz* configuration at different R6G concentrations upon 500 nm excitation. Although these profiles are qualitatively similar to those measured with 530 pump pulses (Figure 6), it is evident that the relative amplitude of the positive component is substantially smaller. This component is hardly visible from 0.5 mM, whereas upon 530 nm excitation its amplitude is larger than or equal to that of the negative component up to 1 mM. This observation clearly confirms that this positive feature originates from the excitation of R6G monomers and reflects the excited-state population decay upon EET quenching by the aggregates.

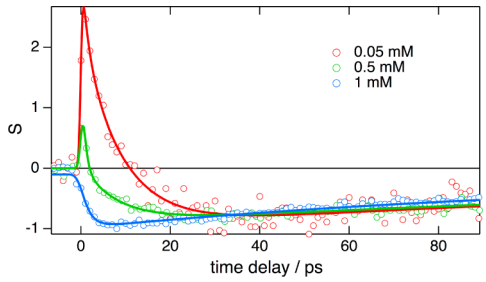

Figure 8. TR-SSHG profiles measured at 400 nm with R6G at the dodecane/water interface upon 500 nm excitation and best multiexponential fits (solid lines).

CONCLUSIONS

The investigation presented here reveals that the photophysics of the widely used dye R6G at a liquid/liquid interface does not intrinsically differ from that in bulk solutions, although the dynamics observed in both environments are apparently very dissimilar. R6G exists in both monomeric and aggregated forms depending on the concentration. Both species can be distinguished using stationary and transient electronic absorption spectroscopy. Our measurements showed that the excited-state lifetime of the aggregates, mostly dimers, amounts to ca. 70 ps, whereas that of the monomers is strongly concentration dependent because of the occurrence of efficient excitation energy transfer to aggregates as already reported previously. The population dynamics observed at the dodecane/water interface is much faster, not because of the occurrence of new deactivation channels but because of the high interfacial R6G concentration. The latter can be explained by the structure of this dye with a charged oxazine unit and a rather lipophilic phenyl substituent. This high interfacial concentration leads to a very efficient quenching of the monomers excited state. Similarly fast quenching in aqueous solution would require concentrations that are beyond the solubility of R6G in water.

This investigation also illustrates an interesting application of liquid interfaces as "microreactors" for investigating intermolecular processes, such as aggregation, that would be highly improbable in bulk solutions unless using unrealistically large reactant concentrations. Better understanding of the excited-state properties of aggregates is important for a large variety of applications, like e.g. in the ink and textile industries[72,73] or the solar cell technology.[74−76]

ASSOCIATED CONTENT

Supporting Information

Original transient absorption spectra measured with R6G in water upon 500 and 530 nm excitation; TCSPC fluorescence decays; wavelength dependence of the relative amplitudes obtained from multiexponential analysis of the TR-SSHG profiles; TR-SSHG profiles measured at the dodecane/water interface in the *xxz* configuration at 400 nm upon 530 nm excitation at low bulk concentrations. This material is available free of charge via the Internet at http://pubs.acs.org.

AUTHOR INFORMATION

Corresponding Author

*E-mail eric.vauthey@unige.ch (E.V.).

Notes

The authors declare no competing financial interest.

ACKNOWLEDGMENTS

This work was supported by the Swiss National Science Foundation through project no. 200020-147098.

REFERENCES

(1) Volkov, A. G. E. *Liquid Interfaces in Chemical, Biological, and Pharmaceutical Applications*; Marcel Dekker: New York, 2009.
(2) Watarai, H.; Teramae, N.; Sawada, T. *Interfacial Nanochemistry*; Kluwer Academic: New York, 2005.
(3) Adamson, A. W.; Gast, A. P. *Physical Chemistry of Surfaces*, 6th ed.; Wiley: New York, 1997.
(4) Eisenthal, K. B. Liquid Interfaces. *Acc. Chem. Res.* **1993**, *26*, 636−43.
(5) Bain, C. D. Sum Frequency Vibrational Spectroscopy of the Solid/Liquid Interface. *J. Chem. Soc., Faraday Trans.* **1995**, *91*, 1281−1296.
(6) Eisenthal, K. B. Liquid Interfaces Probed by Second-Harmonic and Sum-Frequency Spectroscopy. *Chem. Rev.* **1996**, *96*, 1343−1360.
(7) Zhang, Z.; Tsuyumoto, I.; Takahashi, S.; Kitamori, T.; Sawada, T. Monitoring of Molecular Collective Behavior at a Liquid/Liquid Interface by a Time-Resolved Quasi-Elastic Laser Scattering Method. *J. Phys. Chem. A* **1997**, *101*, 4163−4166.
(8) Ikeda, S.; Katayama, K.; Tanaka, T.; Sawada, T.; Tsuyumoto, I.; Harata, A. Generation and Observation of GHz Ultrasonic Waves on Liquid Surfaces and a Liquid/Liquid Interface by Transient Reflecting Grating Method. *J. Chem. Phys.* **1999**, *111*, 9393−9397.
(9) Miranda, P. B.; Shen, Y. R. Liquid Interfaces: A Study by Sum-Frequency Vibrational Spectroscopy. *J. Phys. Chem. B* **1999**, *103*, 3292−3307.
(10) Bowers, J.; Zarbakhsh, A.; Webster, J. R. P.; Hutching, L. R.; Richards, R. W. Neutron Reflectivity Studies at Liquid-Liquid Interfaces: Methodology and Analysis. *Langmuir* **2001**, *17*, 140−145.
(11) Ishizaka, S.; Kim, H. B.; Kitamura, N. Time-Resolved Total Internal Reflection Fluorometry Study on Polarity at a Liquid/Liquid Interface. *Anal. Chem.* **2001**, *73*, 2421−2428.
(12) Richmond, G. L. Molecular Bonding and Interactions at Aqueous Surfaces as Probed by Vibrational Sum Frequency Spectroscopy. *Chem. Rev.* **2002**, *102*, 2693−2724.
(13) De Serio, M.; Bader, A. N.; Heule, M.; Zenobi, R.; Deckert, V. A Near-Field Optical Method for Probing Liquid-Liquid Interfaces. *Chem. Phys. Lett.* **2003**, *380*, 47−53.
(14) Fujiwara, K.; Watarai, H. Total Internal Reflection Resonance Raman Microspectroscopy for the Liquid/Liquid Interface. Ion-Association Adsorption of Cationic Mn(III) Porphine. *Langmuir* **2003**, *19*, 2658−2664.

(15) Liu, D.; Ma, G.; Levering, L. M.; Allen, H. C. Vibrational Spectroscopy of Aqueous Sodium Halide Solutions and Air−Liquid Interfaces: Observation of Increased Interfacial Depth. *J. Phys. Chem. B* **2004**, *108*, 2252−2260.
(16) Brodard, P.; Vauthey, E. Application of Transient Evanescent Grating Technique to the Study of Liquid/Liquid Interfaces. *J. Phys. Chem. B* **2005**, *109*, 4668−4678.
(17) Pant, D.; Girault, H. H. Time-Resolved Total Internal Reflection Fluorescence Spectroscopy. Part I. Photophysics of Coumarin 343 at Liquid/Liquid interface. *Phys. Chem. Chem. Phys.* **2005**, *7*, 3457−3463.
(18) Bordenyuk, A. N.; Benderskii, A. V. Spectrally- and Time-Resolved Vibrational Surface Spectroscopy: Ultrafast Hydrogen-Bonding Dynamics at D_2O/CaF_2 Interface. *J. Chem. Phys.* **2005**, *122*, 134713.
(19) Fujiyoshi, S.; Ishibashi, T.-A.; Onishi, H. Molecular Vibrations at a Liquid-Liquid Interface Observed by Fourth-Order Raman Spectroscopy. *J. Phys. Chem. B* **2006**, *110*, 9571−9578.
(20) Baldelli, S. Surface Structure at the Ionic Liquid-Electrified Metal Interface. *Acc. Chem. Res.* **2008**, *41*, 421−431.
(21) Sekiguchi, K.; Yamaguchi, S.; Tahara, T. Femtosecond Time-Resolved Electronic Sum-Frequency Generation Spectroscopy: A New Method to Investigate Ultrafast Dynamics at Liquid Interfaces. *J. Chem. Phys.* **2008**, *128*, 114715.
(22) Eftekhari-Bafrooei, A.; Borguet, E. Effect of Electric Fields on the Ultrafast Vibrational Relaxation of Water at a Charged Solid-Liquid Interface as Probed by Vibrational Sum Frequency Generation. *J. Phys. Chem. Lett.* **2011**, *2*, 1353−1358.
(23) Zhang, Z.; Piatkowski, L.; Bakker, H. J.; Bonn, M. Ultrafast Vibrational Energy Transfer at the Water/Air Interface Revealed by Two-Dimensional Surface Vibrational Spectroscopy. *Nat. Chem.* **2011**, *3*, 888−893.
(24) Richert, S.; Fedoseeva, M.; Vauthey, E. Ultrafast Photoinduced Dynamics at Air/Liquid and Liquid/Liquid Interfaces. *J. Phys. Chem. Lett.* **2012**, *3*, 1635−1642.
(25) Steel, W. H.; Walker, R. A. Measuring Dipolar Width across Liquid-Liquid Interfaces with 'Molecular Rulers'. *Nature* **2003**, *424*, 296−299.
(26) Scatena, L. F.; Brown, M. G.; Richmond, G. L. Water at Hydrophobic Surfaces: Weak Hydrogen Bonding and Strong Orientation Effects. *Science* **2001**, *292*, 908−912.
(27) Benjamin, I. Molecular Structure and Dynamics at Liquid-Liquid Interfaces. *Annu. Rev. Phys. Chem.* **1997**, *48*, 407−451.
(28) Jungwirth, P.; Tobias, D. J. Specific Ion Effects at the Air/Water Interface. *Chem. Rev.* **2006**, *106*, 1259−1281.
(29) Jedlovszky, P.; Vincze, A.; Horvai, G. Properties of Water/Apolar Interfaces as Seen from Monte Carlo Simulations. *J. Mol. Liq.* **2004**, *109*, 99−108.
(30) Beierlein, F.; Krause, A.; Jaeger, C. M.; Fita, P.; Vauthey, E.; Clark, T. Molecular-Dynamics Simulations of Liquid Phase Interfaces: Understanding the Structure of the Glycerol/Water-Dodecane System. *Langmuir* **2013**, *29*, 11898−11907.
(31) Richmond, G. L. Molecular Bonding and Interactions at Aqueous Surfaces as Probed by Vibrational Sum Frequency Spectroscopy. *Chem. Rev.* **2002**, *102*, 2693−2724.
(32) Fedoseeva, M.; Richert, S.; Vauthey, E. Excited-State Dynamics of Organic Dyes at Liquid-Liquid Interfaces. *Langmuir* **2012**, *28*, 11291−11301.
(33) Carr, C. M. *Chemistry of the Textiles Industry*; Chapman & Hall: London, 1995.
(34) Park, J.-Y.; Hirata, Y.; Hamada, K. Dye Aggregation and Interaction of Dyes with a Water-Soluble Polymer in Ink-Jet Ink for Textiles. *Color. Technol.* **2012**, *128*, 184−191.
(35) Sens, R.; Drexhage, K. H. Fluorescence Quantum Yield of Oxazine and Carbazine Laser Dyes. *J. Lumin.* **1981**, *24*−*25*, 709−12.
(36) Mandalà, M.; Serck-Hanssen, G.; Martino, G.; Helle, K. B. The Fluorescent Cationic Dye Rhodamine 6G as a Probe for Membrane Potential in Bovine Aortic Endothelial Cells. *Anal. Biochem.* **1999**, *274*, 1−6.
(37) Alfano, R. R.; Shapiro, S. L.; Yu, W. Effect of Soap on the Fluorescent Lifetime and Quantum Yield of Rhodamine 6G in Water. *Opt. Commun.* **1973**, *7*, 191−192.
(38) Penzkofer, A.; Lu, Y. Fluorescence Quenching of Rhodamine 6G in Methanol at High Concentration. *Chem. Phys.* **1986**, *103*, 399−405.
(39) Arbeloa, F. L.; Ojeda, P. R.; Arbeloa, I. L. Dimerization and Trimerization of Rhodamine 6G in Aqueous Solution. Effect on the Fluorescence Quantum Yield. *J. Chem. Soc., Faraday Trans. 2* **1988**, *84*, 1903−1912.
(40) Penzkofer, A.; Leupacher, W. Fluorescence Behaviour of Highly Concentrated Rhodamine 6G Solutions. *J. Lumin.* **1987**, *37*, 61−72.
(41) Ilich, P.; Mishra, P. K.; Macura, S.; Burghardt, T. P. Direct Observation of Rhodamine Dimer Structures in Water. *Spectrochim. Acta, Part A* **1996**, *52*, 1323−1330.
(42) Toptygin, D.; Packard, B. Z.; Brand, L. Resolution of Absorption Spectra of Rhodamine 6G Aggregates in Aqueous Solution Using the Law of Mass Action. *Chem. Phys. Lett.* **1997**, *277*, 430−435.
(43) Blom, H.; Chmyrov, A.; Hassler, K.; Davis, L. M.; Widengren, J. Triplet-State Investigations of Fluorescent Dyes at Dielectric Interfaces Using Total Internal Reflection Fluorescence Correlation Spectroscopy. *J. Phys. Chem. A* **2009**, *113*, 5554−5566.
(44) Wu, D.; Deng, G.-H.; Guo, Y.; Wang, H.-f. Observation of the Interference between the Intramolecular IR−Visible and Visible−IR Processes in the Doubly Resonant Sum Frequency Generation Vibrational Spectroscopy of Rhodamine 6G Adsorbed at the Air/Water Interface. *J. Phys. Chem. A* **2009**, *113*, 6058−6063.
(45) Greef, R.; Frey, J. G.; Robinson, J.; Danos, L. Adsorption of Rhodamine 6G at the Water-Air Interface. *Phys. Status Solidi C* **2008**, *5*, 1187−1189.
(46) Chen, Z.; Tang, Y.-J.; Xie, T.-T.; Chen, Y.; Li, Y.-Q. Fluorescence Spectral Properties of Rhodamine 6G at the Silica/Water Interface. *J. Fluoresc.* **2008**, *18*, 93−100.
(47) Zheng, X.-Y.; Harata, A.; Ogawa, T. Study of the Adsorptive Behavior of Water-Soluble Dye Molecules (Rhodamine 6G) at the Air−Water Interface using Confocal Fluorescence Microscope. *Spectrochim. Acta, Part A* **2001**, *57*, 315−322.
(48) Meech, S. R.; Yoshihara, K. Picosecond Dynamics at the Solid—Liquid Interface: a Total Internal Reflection Time-Resolved Surface Second-Harmonic Generation Study. *Chem. Phys. Lett.* **1990**, *174*, 423−427.
(49) Castro, A.; Sitzmann, E. V.; Zhang, D.; Eisenthal, K. B. Rotational Relaxation at the Air/Water Interface by Time-Resolved Second Harmonic Generation. *J. Phys. Chem.* **1991**, *95*, 6752−6753.
(50) Brodard, P.; Vauthey, E. Exploring Liquid/Liquid Interfaces with Transient Evanescent Grating Techniques. *Rev. Sci. Instrum.* **2003**, *74*, 725−728.
(51) Punzi, A.; Brodard, P.; Vauthey, E. Transient Grating Investigations at Liquid/Liquid Interfaces. *Chimia* **2005**, *59*, 116−118.
(52) Axelrod, D.; Hellen, E. H.; Fulbright, R. M. Total Internal Reflection Fluorescence. *Top. Fluoresc. Spectrosc.* **1992**, *3*, 289−343.
(53) Muller, P.-A.; Högemann, C.; Allonas, X.; Jacques, P.; Vauthey, E. Deuterium Isotope Effect on the Charge Recombination Dynamics of Contact Ion Pairs Formed by Electron Transfer Quenching in Acetonitrile. *Chem. Phys. Lett.* **2000**, *326*, 321−327.
(54) Furstenberg, A.; Vauthey, E. Ultrafast Excited-State Dynamics of Oxazole Yellow DNA Intercalators. *J. Phys. Chem. B* **2007**, *111*, 12610−12620.
(55) Duvanel, G.; Banerji, N.; Vauthey, E. Excited-State Dynamics of Donor-Acceptor Bridged Systems Containing a Boron-Dipyrromethene Chromophore: Interplay between Charge Separation and Reorientational Motion. *J. Phys. Chem. A* **2007**, *111*, 5361−5369.
(56) Banerji, N.; Duvanel, G.; Perez-Velasco, A.; Maity, S.; Sakai, N.; Matile, S.; Vauthey, E. Excited-State Dynamics of Hybrid Multichromophoric Systems: Toward an Excitation Wavelength

Control of the Charge Separation Pathways. *J. Phys. Chem. A* **2009**, *113*, 8202−8212.
(57) Fita, P.; Luzina, E.; Dziembowska, T.; Radzewicz, C.; Grabowska, A. Chemistry, Photophysics, and Ultrafast Kinetics of Two Structurally Related Schiff Bases Containing the Naphthalene or Quinoline Ring. *J. Chem. Phys.* **2006**, *125*, 184508.
(58) Punzi, A.; Martin-Gassin, G.; Grilj, J.; Vauthey, E. Effect of Salt on the Excited-State Dynamics of Malachite Green in Bulk Aqueous Solutions and at Air/Water Interfaces: a Femtosecond Transient Absorption and Surface Second Harmonic Generation Study. *J. Phys. Chem. C* **2009**, *113*, 11822−11829.
(59) Fita, P.; Fedoseeva, M.; Vauthey, E. Hydrogen-Bond-Assisted Excited-State Deactivation at Liquid/Water Interfaces. *Langmuir* **2011**, *27*, 4645−4652.
(60) Fedoseeva, M.; Fita, P.; Vauthey, E. Excited-State Dynamics of Charged Dyes at Alkane/Water Interfaces in the Presence of Salts and Ionic Surfactants. *Langmuir* **2013**, *29*, 14865−14872.
(61) Brevet, P.-F. *Surface Second Harmonic Generation*; Presses polytechniques et universitaires romandes: Lausanne, 1997.
(62) Milojevich, C. B.; Silverstein, D. W.; Jensen, L.; Camden, J. P. Surface-Enhanced Hyper-Raman Scattering Elucidates the Two-Photon Absorption Spectrum of Rhodamine 6G. *J. Phys. Chem. C* **2013**, *117*, 3046−3054.
(63) Makarov, N. S.; Drobizhev, M.; Rebane, A. Two-Photon Absorption Standards in the 550−1600 nm Excitation Wavelength Range. *Opt. Express* **2008**, *16*, 4029−4047.
(64) Moreno-Villoslada, I.; Fuenzalida, J. P.; Tripailaf, G.; Araya-Hermosilla, R.; Pizarro, G. d. C.; Marambio, O. G.; Nishide, H. Comparative Study of the Self-Aggregation of Rhodamine 6G in the Presence of Poly(sodium 4-styrenesulfonate), Poly(N-phenylmaleimide-co-acrylic acid), Poly(styrene-alt-maleic acid), and Poly(sodium acrylate). *J. Phys. Chem. B* **2010**, *114*, 11983−11992.
(65) Burshtein, A. I. Non-Markovian Theories of Transfer Reactions in Luminescence and Chemiluminescence and Photo- and Electrochemistry. *Adv. Chem. Phys.* **2004**, *129*, 105−418.
(66) Deshpande, A. V.; Beidoun, A.; Penzkofer, A.; Wagenblast, G. Absorption and Emission Spectroscopic Investigation of Cyanovinyldiethylaniline Dye Vapors. *Chem. Phys.* **1990**, *142*, 123−131.
(67) Smirl, A. L.; Clark, J. B.; Van Stryland, E. W.; Russell, B. R. Population and Rotational Kinetics of the Rhodamine B Monomer and Dimer: Picosecond Transient Spectrometry. *J. Chem. Phys.* **1982**, *77*, 631−640.
(68) Högemann, C.; Vauthey, E. Investigation of the Competition between Electron and Energy Transfer in the Quenching of Aromatic Ketones in the Triplet State Using Picosecond Transient Grating Spectroscopy. *J. Phys. Chem. A* **1998**, *102*, 10051−10059.
(69) Zimdars, D.; Dadap, J. I.; Eisenthal, K. B.; Heinz, T. F. Anisotropic Orientational Motion of Molecular Adsorbates at the Air-Water Interface. *J. Phys. Chem. B* **1999**, *103*, 3425−3433.
(70) Tamai, N.; Yamazaki, T.; Yamazaki, I.; Mizuma, A.; Mataga, N. Excitation Energy Transfer between Dye Molecules Absorbed on Vesicle Surface. *J. Phys. Chem.* **1987**, *91*, 3503−3508.
(71) Sitzmann, E. V.; Eisenthal, K. B. Dynamics of Intermolecular Electronic Energy Transfer at an Air/Liquid Interface. *J. Chem. Phys.* **1989**, *90*, 2831−2832.
(72) Blank, K.-H. Textile Printing - Conventional and Digital. *Textilveredlung* **2004**, *39*, 6−8.
(73) Ridgway, C. J.; Gane, P. A. C. Controlling the Absorption Dynamic of Water-Based Ink into Porous Pigmented Coating Structures to Enhance Print Performance. *Nord. Pulp Paper Res.* **2002**, *17*.
(74) Beckers, E. H. A.; Meskers, S. C. J.; Schenning, A. P. H. J.; Chen, Z.; Wuerthner, F.; Marsal, P.; Beljonne, D.; Cornil, J.; Janssen, R. A. J. Influence of Intermolecular Orientation on the Photoinduced Charge Transfer Kinetics in Self-Assembled Aggregates of Donor-Acceptor Arrays. *J. Am. Chem. Soc.* **2006**, *128*, 649−657.
(75) Koops, S. E.; O'Regan, B. C.; Barnes, P. R. F. Parameters Influencing the Efficiency of Electron Injection in Dye-Sensitized Solar Cells. *J. Am. Chem. Soc.* **2009**, *131*, 4808−4818.
(76) Khazraji, A. C.; Hotchandani, S.; Das, S.; Kamat, P. V. Controlling Dye (Merocyanine-540) Aggregation on Nanostructured TiO_2 Films. An Organized Assembly Approach for Enhancing the Efficiency of Photosensitization. *J. Phys. Chem. B* **1999**, *103*.